Volume 1 | Number 1 | Jan 2013 | Pages 1–100

Soft Matter

www.rsc.org/softmatter

ROYAL SOCIETY
OF CHEMISTRY

www.rsc.org/softmatter

Interplay of particle shape and suspension properties: A study of cube-like particles[†,‡]

Debra J. Audus,[*a] **Ahmed M. Hassan,**[a] **Edward J. Garboczi,**[b] **and Jack F. Douglas**[*a]

With advances in anisotropic particle synthesis, particle shape is now a feasible parameter for tuning suspension properties. However, there is a need to determine how these newly synthesized particles with prescribed shapes affect suspension properties and to solve the inverse problem of inferring the shape of particles from property measurements. Either way, accurate suspension property predictions are required. Towards this end, we calculated a set of dilute suspension properties for a family of cube-like shapes that smoothly interpolate between spheres and cubes. Using three conceptually different methods, we numerically computed the electrical properties of particle suspensions, including the intrinsic conductivity of perfect conductors and insulators. We also considered hydrodynamic properties relevant to particle solutions including the hydrodynamic radius, the intrinsic viscosity and the intrinsic solvent diffusivity. Additionally, we determined the second osmotic virial coefficient using analytic expressions along with numerical integration. As the particles became more cube-like, we found that all of the properties investigated become more sensitive to particle shape.

1 Introduction

In the past two decades, there has been significant progress in the synthesis of anisotropic particles,[1–13] making it possible to create particles with unique shapes such as stars,[11] cages,[12] nanocubes,[12] nanorods,[5] and red blood cell mimics.[13] These advances in synthesis lead to new possibilities for applications where particle shape is important, including optics[14] and drug delivery.[15] However, much work needs to be done to fully characterize the effect of particle shape on material properties. Due to the diversity of possible shapes, simulation methods can potentially play an important role in the characterization of theses particles. For example, Damasceno *et al.*[16] predicted self-assembled structures of 145 different polyhedra. However, particle self-assembly is not the only phenomenon of interest. How these particles affect transport properties of solutions and electrical properties of composite materials, along with methods for solving the inverse problem, i.e., using properties to characterize particle shape, is important. In particular, the inverse problem has a long history in the polymer science[17,18] and protein communities.[19] Thus, we have investigated the dilute suspension properties of a fam-
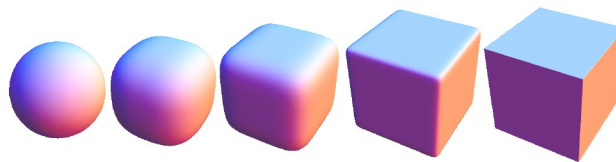
Fig. 1 Examples of superballs whose surface by definition corresponds to $|x|^{2s} + |y|^{2s} + |z|^{2s} = a^{2s}$. From left to right the s values are 1, 1.5, 2.5, 10 and ∞

ily of simple but non-analytically solvable cube-like shapes, which are convex particles that smoothly interpolate between spheres and cubes as can been seen in Fig. 1.

The surface of these cube-like particles, also known as superballs, can be simply described by an extension of the equation for a sphere,[20]

$$|x|^{2s} + |y|^{2s} + |z|^{2s} = a^{2s}, \qquad (1)$$

where s is a parameter that can vary between one and infinity corresponding to a sphere and a cube, respectively, and a is a measure of size. In the case of a sphere, a is the radius, and for a cube, a is half the edge length. In 2011, the first particle of this class with an intermediate value of s was synthesized,[21] μm-sized hollow silica particles with a s value of roughly 1.8. Prior to synthetic developments, the packing[22] and phase behavior[23,24] of these objects was investigated computationally. Since then the freezing of cubes with rounded edges, a similar system, has also been studied computationally.[25] Although

there have been several studies of the electrical and transport properties of suspensions of spheres and cubes,[26–32] to our knowledge there has not yet been any study for intermediate values of s, which led us to investigate the dilute suspension properties of these cube-like particles.

2 Properties of interest and an electrostatic-hydrodynamic analogy

Three electrical properties are of central interest in connection to material science applications and particle shape characterization, namely, the self-capacitance C, the intrinsic conductivity for a perfect conductor $[\sigma]_\infty$, and the intrinsic conductivity for a perfect insulator $[\sigma]_0$. Each property has an associated variational principle as a function of shape. It has been rigorously shown that these shape functionals are minimized by the sphere for all particles having fixed volume.[33] While these shape functionals are widely appreciated as fundamental metrics of shape, their utility has previously been limited by the difficulty of calculating these quantities accurately.[33,34]

Of these three quantities, the latter two are of direct interest for composites since they both represent the second virial coefficients for the conductivity of the system, which can be expressed as

$$\sigma/\sigma_0 = 1 + [\sigma]\phi + \mathcal{O}(\phi^2) \tag{2}$$

where σ is the conductivity of the entire system with volume fraction ϕ randomly oriented, solid particles of a given shape embedded in the matrix with a conductivity of σ_0. The intrinsic conductivity $[\sigma]$, in general, depends on the ratio of the conductivity of the inclusions to the matrix and the particle shape. The two contrast limiting conditions are perfect conducting particles and perfect insulating particles, which reduce $[\sigma]$ to $[\sigma]_\infty$ and $[\sigma]_0$, respectively. Mathematically, all three electrical properties can be computed by first solving Laplace's equation with either Dirchelet (C and $[\sigma]_\infty$) or Neumann ($[\sigma]_0$) boundary conditions on the particle and then solving functionals of the potential at the surface of the particle.[35] Although absolutely perfect conductors (superconductors) and perfect insulators do not exist, these limiting cases are often useful idealizations in practice since the contrast, the ratio of the conductivities of the inclusions to the matrix, is often large. Note that due to the correspondence between electrostatics and heat transfer,[32] the intrinsic electrical conductivity is equivalent to the intrinsic thermal conductivity, which has recently been studied for various shapes experimentally, computationally, and theoretically by Martin and coworkers.[36,37]

In addition to electrical properties, we were also interested in hydrodynamic properties relevant to solutions, specifically, the hydrodynamic radius R_h of a Brownian particle, the intrinsic viscosity $[\eta]$, and the intrinsic solvent diffusivity $[D_s]$. This is the standard set of properties, along the second osmotic

virial coefficient B_{22}, normally considered in macromolecular characterization, and thus form a useful set to study particles.[17,18] The three hydrodynamic properties satisfy the following equations.

$$D = \frac{k_B T}{6\pi\eta_0 R_h} \tag{3}$$

where D is the diffusion coefficient of the particle, k_B is Boltzmann's constant, T is the temperature and η_0 is the viscosity of the solvent.

$$\frac{\eta}{\eta_0} = 1 + [\eta]\phi + \mathcal{O}(\phi^2) \tag{4}$$

where η is the visocosity of the solution.

$$\frac{D_s}{D_0} = 1 + [D_s]\phi + \mathcal{O}(\phi^2) \tag{5}$$

where D_s is the diffusion coefficient for the solvent when relatively large, impenetrable particles are present, and D_0 is the diffusion coefficient for the solvent when particles are not present.

In particle as well as polymer characterization measurements, the second osmotic virial coefficient B_{22} is also fundamental as it quantifies the strength of the average interparticle interaction strength in the dilute limit.[38] This quantity is the leading term in the virial expansion for the reduced osmotic pressure Z,

$$Z = 1 + \frac{B_{22}}{V}\phi + \mathcal{O}(\phi^2), \tag{6}$$

where V is the particle volume. B_{22} can be expressed analytically for rigid, non-interacting convex particles[39] and evaluated numerically otherwise.

Due to the mathematical similarities between the equations to solve the electrical properties and those to solve the hydrodynamic properties,[32,40] the electrical properties can be, depending on the property, exactly or approximately related to the hydrodynamic properties relevant to rigid particle solutions. Specifically, $C \approx R_h$, $[\sigma]_\infty \approx q_\eta[\eta]$ and $[\sigma]_0 = [D_s]$ where q_η is a proportionality constant weakly dependent on shape.

In the calculation of R_h from C, the underlying assumptions are that the Reynolds number is low, i.e., inertial effects are not important, that the particles are rigid bodies with a hydrodynamic stick boundary condition, and that the Oseen tensor can be angularly preaveraged. This angular preaveraging assumption is valid if particles explore all orientations in an unbiased way.[41] Physically, the unbiased exploration of orientations is achieved for low Peclet number where diffusion dominates. For high Peclet number where advection dominates, it is still possible to achieve an unbiased exploration of orientations depending on the processing history. Comparison to existing exact hydrodynamic results, high resolution boundary element calculations and additional numerical calculations

for diverse shapes indicate that the relation between R_h and C holds to within an uncertainty on the order of 1 %[40,42] and is exact for triaxial ellipsoids.[41] Thus, this approximation is acceptable for numerical estimates of R_h from C.

The determination of $[\eta]$ from $[\sigma]_\infty$ also involves an angular averaging and the same hydrodynamic boundary conditions. The proportionality constant q_η is determined by first mapping the particle shape to an ellipsoid using the electric polarizabilty tensor, from which $[\sigma]_\infty$ is determined, and then requiring that q_η is exact for that ellipsoid.[43] Since both $[\eta]$ and $[\sigma]_\infty$ are known quantities for this shape, q_η can be determined for any ellipsoid.[32] This construction leads to $[\eta]$ estimates that are in agreement with exact and numerical results to within an uncertainty of 1.5 %,[43] similar to the uncertainty for R_h. In the case of cube-like particles, we take $q_\eta = 6/5$.

$[D_s]$ is exactly equal in magnitude to the average of the diagonal components of the hydrodynamic virtual mass tensor,[32] as well as to $[\sigma]_0$,[35] if the size of the particle is significantly larger than the size of the solvent so that the solvent to be treated as a continuum. Exact values have been calculated for triaxial ellipsoids[30] and a few other shapes.[32]

In addition to these electrostatic-hydrodynamic analogies, there is also a direct relation between C of a particle with a specified shape and the Smoluchowski rate constant k for diffusion-controlled reactions[44] of small particles with diffusion constant D diffusing towards an absorbing, larger particle with the specified shape, specifically, $k = 4\pi DC$. This relation is exact if the particle concentration is dilute, there are no long range interactions, and under steady state conditions.[45]

3 Computational methods

The three electrical properties and, thus, their corresponding hydrodynamic properties were calculated using standard definitions:[32,35,46]

$$C = -\frac{1}{4\pi} \int_\Omega dS\, \hat{\mathbf{n}} \cdot \nabla\Phi, \qquad (7)$$

$$[\sigma]_\infty = \mathrm{Tr}(\alpha_{\mathbf{e}})/(3V) = 1 - \frac{1}{V} \int_\Omega dS\, z\hat{\mathbf{n}} \cdot \nabla\Phi, \qquad (8)$$

$$[\sigma]_0 = \mathrm{Tr}(\alpha_{\mathbf{m}})/(3V) = -1 + \frac{1}{V} \int_\Omega dS\, \hat{\mathbf{k}} \cdot \hat{\mathbf{n}}\, \Phi \qquad (9)$$

where $\alpha_{\mathbf{e}}$ is the electrostatic polarizability tensor, $\alpha_{\mathbf{m}}$ is the magnetic polarizablility tensor, z is the value of the Cartesian coordinate at the surface, $\hat{\mathbf{k}}$ is a vector in the z direction, $\hat{\mathbf{n}}$ is the normal vector of the surface of the object Ω, and the integrations are over the surface of the object. Φ satisfies Laplace's equation outside the object with $\Phi(\mathbf{r}) = 0$ as $\mathbf{r}$ approaches infinity. However, the boundary conditions on the surface Ω are different for each property. Specifically, $\Phi = 1$ for C, $\Phi = z + c$ for $[\sigma]_\infty$ where c is determined such

that $\int_\Omega dS\,\hat{\mathbf{n}} \cdot \nabla\Phi = 0$, and $\hat{\mathbf{n}} \cdot \nabla\Phi = z$ for $[\sigma]_0$. In the above equations, we have made use of the symmetry of the object. Thus, the results are unaffected by both object rotations and displacements.

Three different methods were used to solve Eqs. 7-9. The first computational method was ZENO,[47] a numerical path-integration method that can be used to solve for C and $[\sigma]_\infty$ (Eqs. 7 and 8). This method involved placing the object, in this case, a cube-like particle, inside an enclosing sphere and then launching random walks from the surface of the sphere. The fraction of walks that hit the object as opposed to going to infinity can be directly related to C. If additionally, random charges for the x, y, and z directions were assigned to each walk, counters could be kept that allow one to compute $\alpha_{\mathbf{e}}$ and thus $[\sigma]_\infty$ via Eq. 8.[40] For this method, the object was represented exactly since the shape is known, and specific details of the modifications to the ZENO code available online can be found in the ESI†. For each shape, a skin thickness of 10^{-4} was used, and the results of ten runs of one million walks were averaged.

The second computational method was COMSOL Multiphysics,[48] a commercial finite element package.[49] This method involved creating a finite element mesh of both the object and the surroundings in which the object is embedded. Then the Laplace equation was solved with the relevant boundary conditions, and the desired quantities were computed via Eqs. 8 and 9. Ideally, the surroundings would extend to infinity but this would require an infinite mesh, a computationally infeasible requirement. Hence, the object to be simulated in COMSOL was embedded in a sphere whose radius R_0 was increased until the calculated properties converged; the polarizability values were found to converge when R_0 was larger than 25 times the radius of the object. However, the capacitance was slow to converge and required R_0 of at least 120 times larger than the radius of the object of interest. Similar slow convergence, with respect to R_0, has previously been reported in a finite element calculation of the self-capacitance of a cube.[27] For all values of s simulated, COMSOL computed the mesh with the requirement that the maximum finite element size is 0.025 inside the cube-like particle with $a = 1$. The mesh was allowed to progressively increase outside of the object in the surrounding sphere of radius R_0. Special care has to be taken for calculations of $[\sigma]_\infty$ for the cube due to its sharp corners. Only in this case, the volumetric representation of Eq. 8, reported as Eq. 7 in Ref. 29, is employed, which yielded more accurate results than Eq. 8 at a significantly lower meshing resolution. Another alternative for high accuracy would be to follow the approach of Martin et al.[50]

The third computational method was SCUFF-EM,[51] a boundary element method that only requires meshing of the surface of the object. The surface mesh was generated by placing nodes on the surface of object uniformly in the po-
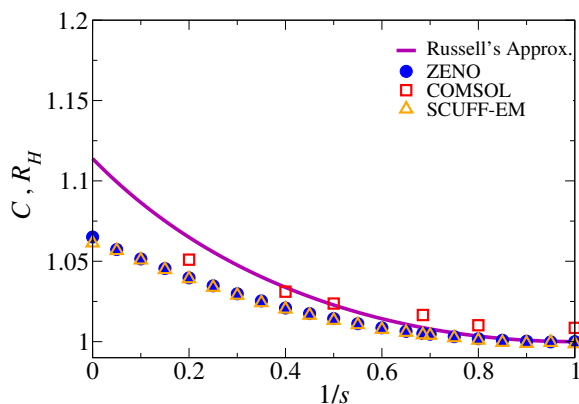
Fig. 2 Self-capacitance C and hydrodynamic radius R_h for cube-like particles. Values are normalized such that all particles have the same volume as a sphere with radius one. Russell approximation[53] is equivalent to a spherical harmonic expansion to first order and is discussed in Appendix B.

Fig. 3 Five sixths of the intrinsic conductivity of a perfect conductor $[\sigma]_\infty$ and $[\eta]$ for cube-like particles.
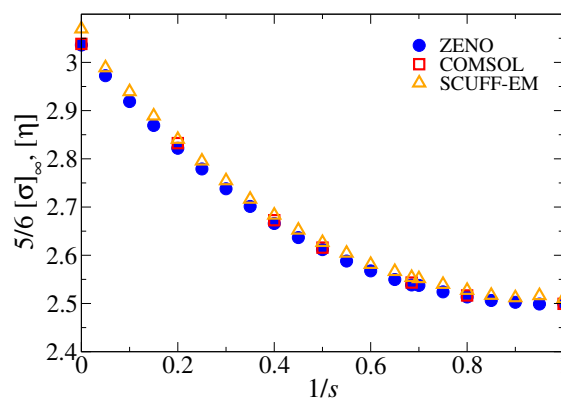
lar and azimuthal angles with additional nodes placed at the top and bottom of the object. Using this scheme, the mesh was generated by connecting the 6,962 nodes using triangles as shown in the ESI†. The same number of nodes and meshing scheme was used for all values of s, and the results were invariant when more nodes were added to the surface of the object indicating that 6,962 nodes were sufficient for the accurate calculation of the properties of the cube-like particles.

Additionally, B_{22} for cube-like particles with a purely repulsive hard core excluded volume interaction was calculated by the exact relation from integral geometry $RS + V$ for convex particles where R is the integral of mean curvature, S is the surface area, and V is the volume of the object.[39] Since there is an analytic expression for the surface of the cube-like particles, each of the three quantities could be written in integral form and then numerically integrated with Mathematica,[52] commercial software,[49] to solve the desired equation. The expressions for these quantities can be found in Appendix A.

4 Results and discussion

4.1 Predictions

The self-capacitance C and its near equivalent, the hydrodynamic radius R_h, were calculated for cube-like particles using ZENO and SCUFF-EM as seen in Fig. 2. The results for COMSOL are unlikely to be accurate due to challenges associated with convergence[27] as discussed in Section 3. R_h is a particularly important quantity since it is inversely propor-

tional to the self-diffusion coefficient via the Stokes-Einstein relation (see Eq. 3). We found for cube-like particles with identical volumes that R_h increases as s increases with only a marginal (6 %) change in value for the limiting case of a cube so that the self-diffusion coefficient is only minimally affected by shape. This result is somewhat surprising since the radius of a sphere that circumscribes a cube with a volume equal to $4\pi/3$ is roughly 1.4.

Given the small change in R_h, we directly compared our predictions to Russell's approximation[53] (see Appendix B), which is a spherical harmonic expansion to first order and is equivalent to $R_h = [S/(4\pi)]^{1/2}$. Since we have the values for the surface area as a function of s, R_h could easily be approximated. However, we found that this approximation is only useful when the particles were nearly spherical limiting its applicability.

We also computed the intrinsic conductivity of a perfect conductor $[\sigma]_\infty$ and the intrinsic viscosity $[\eta]$, as can be seen in Fig. 3. For a sphere ($s = 1$), $[\eta] = 2.5$, the well known result of Einstein.[31] For a cube, our predictions were in line with previous numerical estimates[28,29,54,55] and measured results.[56] Both $[\sigma]_\infty$ and $[\eta]$ were significantly more sensitive to the particle shape than R_h. This change was equivalent to a 20 % increase in the value as particles go from spheres to cubes. Thus, the shape can be used to tune the properties. Conversely, if the value of s is unknown, these properties could be measured to estimate s especially at large s where the results were more sensitive. For $[\eta]$, this sensitivity is likely a consequence of increased drag on the corners.

Figure 4 shows the prediction for the intrinsic conductivity of a perfect insulator $[\sigma]_0$, as well as the intrinsic solvent diffusivity $[D_s]$. As previously mentioned, both of these quan-
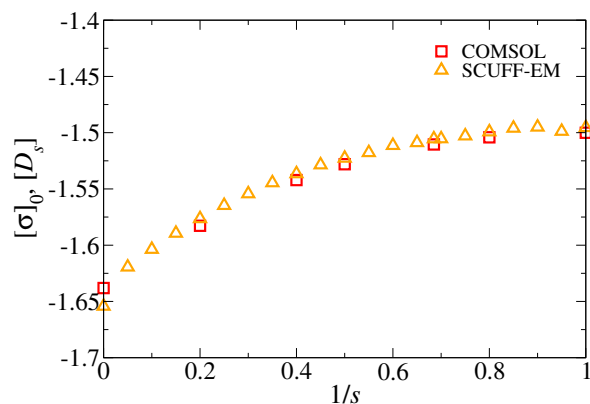
Fig. 4 Intrinsic conductivity of a perfect insulator $[\sigma]_0$ and the intrinsic solvent diffusivity $[D_s]$ for cube-like particles.

Fig. 5 Second osmotic virial coefficient B_{22} normalized by volume for cube-like particles. Symbols correspond to quantities calculated by Batten *et al.* [23] using a Monte Carlo method.

tities are related to the hydrodynamic virtual mass tensor, [32,35] and have been shown to be equal to negative three halves for a sphere. [30] This is in excellent agreement with the results. Also, the COMSOL result for the cube is in line with previous calculations. [29] In terms of sensitivity, both $[\sigma]_0$ and $[D_s]$ were less sensitive to shape than $[\eta]$ but more sensitive than R_h. This sensitivity can be quantified by the increase in value as the particles go from spheres to cubes, which is roughly 8 %. For similar reasons to those for $[\eta]$, namely the corners inhibit flow, $[D_s]$ and thus $[\sigma]_0$ are smaller for a cube than a sphere.

In order to compute the properties of cube-like suspensions, we used three different computational methods, each of which is based on a different algorithm. We found that all three methods were in agreement with the exception of C when the finite element method was used where the slow convergence with respect to mesh size and R_0 is well known. [27] Thus, this problem could probably be overcome by optimizing the meshing scheme and/or increasing R_0. Such improvements are beyond the scope of our work. Nonetheless, the general agreement suggests that the scatter in the data is representative of the uncertainty. We also compared the computational resources required for the three algorithms and found that they were generally comparable. Details can be found in the ESI†.

The second osmotic virial coefficient B_{22} for hard cube-like particles was computed using numerical integration. The results can be seen in Fig. 5. We directly compared our results with those of Batten *et al.*, [23] who used a Monte Carlo method along with a more general expression for B_{22}. We found excellent agreement between the values of s that were considered by Ref. 23 and also found that numerical integration allowed us to compute values for values of s that were difficult to access with this Monte Carlo method. Such a challenge arises from
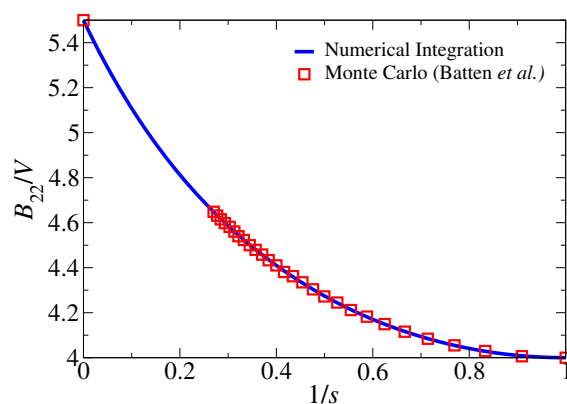
trying to determine if two almost, but not quite, cube-shaped particles overlap. However, the Monte Carlo method has the advantage that it can be easily adapted to compute higher virial coefficients or to include more complicated pair-wise interactions for B_{22}. [57]

B_{22} increased with increasing s, which by definition implied that the osmotic pressure would be higher for particles that are more cube-like than those that are more sphere-like. We also found that the change in the value of B_{22} was large enough that, in principal, it could be used as a metric in order to measure the value of s of a dilute suspension of cube-like particles. However, unlike $[\eta]$ and $[D_s]$, it depends on interparticle interactions thus if the synthesized particles had any interactions other than an infinite overlap penalty, B_{22} would need to be determined using other methods. A better strategy would be to determine s using $[\eta]$ first and then to compare B_{22} with its hard object value to determine the role of interparticle interactions.

4.2 Comparison to experiments

Where possible, we directly compared our results to experiments. [56,58] This comparison is shown in Table 1; we found that all the predictions matched the experimental results within the uncertainty bounds. For $s = 1.4$, $[\eta]$ is quite similar to the value for a sphere, 2.5, such that for the experimental data, the value is the same as a sphere within numerical uncertainty. Note that the experimental Reynold's number was $\mathscr{O}(10^{-11})$, so the approximations in calculating R_h from C as well as $[\eta]$ from $[\sigma]_\infty$ should be valid. Additionally, the particles were composed of silica shells; as long as the shells are rigid, the calculations are unaffected. For s approaching infinity, $[\eta]$ is

noticeably different from that of a sphere.

R_h for $s = 1.4$ was determined by measuring the diffusion coefficient and then using the Stokes-Einstein equation (Eq. 3). This resulted in a value of 0.80 μm $\pm$ 0.06 μm, which could be converted to the normalized units using $s = 1.4$, $a = 0.75$ μm $\pm$ 0.03 μm (see Eq. 1) and the volume of the cube-like particle (see Eq. 11). The resulting R_h was equal to both the sphere and the cube-like particle with $s = 1.4$ within uncertainty, highlighting the lack of sensitivity of the property values for values of s close to those of the sphere.

Table 1 Comparison of predictions to experimental work. Values for $s = 1.4$ are from Royer *et al.*[58] and values for $s \to \infty$ are from Mallavajula *et al.*[56] Details on the calculation of the uncertainties, equivalent to one standard deviation, can be found in the experimental sources.

	s	ZENO	SCUFF-EM	COMSOL	Experiment
$[\eta]$	1.4	2.54	2.55	2.54	2.57 ± 0.11
$[\eta]$	∞	3.04	3.07	2.97	3.1 ± 0.2
R_h	1.4	1.00	1.00	1.02	0.97 ± 0.08

5   Conclusions

We considered three different methods, where possible, to compute the intrinsic conductivity of both perfect conductors and insulators, the hydrodynamic radius, the intrinsic viscosity, and the intrinsic solvent diffusivity of dilute suspensions of cube-like particles. We found that all properties were dependent on the shape but weakly so for more spherical particles. For more cube-like particles, shape can be used to tune the properties or alternatively these properties can be used to characterize particle shape. The latter strategy would be more useful for suspensions of cube-like particles, since the intrinsic viscosity has a greater sensitivity to shape. All the three methods are in agreement and would be useful for future calculations. However, for the capacitance, the system size (R_0) may need to be increased for finite element calculations. We also determined the second osmotic virial coefficient for hard cube-like particles using analytic expressions coupled with numerical integration and found that our results were in excellent agreement with a Monte Carlo method. In the future, we expect the techniques discussed will be applicable to studying other property-shape relationships[59] as well as quantifying shape or individual particle properties.[60] One potential example is the properties of dimers, trimers, and finite linear arrays of superballs. Interestingly, the intrinsic conductivity of perfectly conducting dimers of cubes is actually lower than that for dimers of spheres and the difference in magnitude is much smaller, roughly 1 %.

Appendix A: Volume, surface area, and integral of mean curvature

The radius of the cube-like particle describe by Eq. 1 in spherical coordinates can be represented as

$$r(\theta, \varphi) = a^{2s}(|\cos(\varphi)|^{2s}|\sin(\theta)|^{2s} + |\sin(\varphi)|^{2s}|\sin(\theta)|^{2s} + |\cos(\theta)|^{2s})^{-1/(2s)} \quad (10)$$

where $0 \leq \theta \leq \pi$ and $0 \leq \varphi < 2\pi$. Thus, the volume can be written as

$$V = \frac{8}{3} \int_0^{\pi/2} d\theta \int_0^{\pi/2} d\varphi \sin(\theta) r^3 \quad (11)$$

where the factor of 8 comes from integrating only over the first quadrant due to symmetry. Similarly, if **x** represents a vector from the origin to the surface at a given θ and φ, the surface area becomes

$$S = 8 \int_0^{\pi/2} d\theta \int_0^{\pi/2} d\varphi |\mathbf{x}_\theta \times \mathbf{x}_\varphi| \quad (12)$$

where subscripts represent derivatives. Similarly, the integral of mean curvature is

$$R = \frac{8}{4\pi} \int_0^{\pi/2} d\theta \int_0^{\pi/2} d\varphi \{(\mathbf{x}_\theta \cdot \mathbf{x}_\theta)[(\mathbf{x}_\theta \times \mathbf{x}_\varphi) \cdot \mathbf{x}_{\varphi\varphi}]$$
$$+ (\mathbf{x}_\varphi \cdot \mathbf{x}_\varphi)[(\mathbf{x}_\theta \times \mathbf{x}_\varphi) \cdot \mathbf{x}_{\theta\theta}] - 2(\mathbf{x}_\theta \cdot \mathbf{x}_\varphi)[(\mathbf{x}_\theta \times \mathbf{x}_\varphi) \cdot \mathbf{x}_{\theta\varphi}]\}$$
$$[2(\mathbf{x}_\theta \cdot \mathbf{x}_\theta)(\mathbf{x}_\varphi \cdot \mathbf{x}_\varphi) - 2(\mathbf{x}_\theta \cdot \mathbf{x}_\varphi)^2]^{-1}. \quad (13)$$

Appendix B: Russell's approximation

Russell's approximation[53] can be derived using a spherical harmonic expansion. The radius of the object can be represented as

$$r = a \left(1 + \varepsilon \sum_{k=0}^{\infty} f_k(\theta, \varphi) \right) \quad (14)$$

where a is a coefficient and f_k are spherical harmonics. From Brenner,[61] R_h is

$$R_h = a(1 + \varepsilon f_0) + \mathcal{O}(\varepsilon^2) \quad (15)$$

and the surface area is

$$S = 4\pi a^2 (1 + 2\varepsilon f_0) + \mathcal{O}(\varepsilon^2). \quad (16)$$

Thus, $[S/(4\pi)]^{1/2}$ is equal to R_h upto $\mathscr{O}(\varepsilon)$, a conclusion which had previously observed by Douglas and Freed.[62] This simple approximation is widely utilized in protein dynamics simulations.[63]

Notes and references

1 K. J. Lee, J. Yoon and J. Lahann, *Curr. Opin. Colloid In.*, 2011, **16**, 195–202.

2 S. C. Glotzer and M. J. Solomon, *Nat. Mater.*, 2007, **6**, 557–562.

3 T. K. Sau and A. L. Rogach, *Adv. Mater.*, 2010, **22**, 1781–1804.

4 Y. Yin and a. P. Alivisatos, *Nature*, 2005, **437**, 664–70.

5 V. F. Puntes, K. M. Krishnan and A. P. Alivisatos, *Science*, 2001, **291**, 2115–7.

6 C.-Y. Chiu, Y. Li, L. Ruan, X. Ye, C. B. Murray and Y. Huang, *Nat. Chem.*, 2011, **3**, 393–9.

7 M. Grzelczak, J. Pérez-Juste, P. Mulvaney and L. M. Liz-Marzán, *Chem. Soc. Rev.*, 2008, **37**, 1783–91.

8 L. Manna, E. C. Scher and A. P. Alivisatos, *J. Am. Chem. Soc.*, 2000, **122**, 12700–12706.

9 H. Li, A. G. Kanaras and L. Manna, *Accounts Chem. Res.*, 2013, **46**, 1387–96.

10 S. Kumar and T. Nann, *Small*, 2006, **2**, 316–29.

11 S.-M. Lee, Y.-w. Jun, S.-N. Cho and J. Cheon, *J. Am. Chem. Soc.*, 2002, **124**, 11244–5.

12 S. E. Skrabalak, L. Au, X. Li and Y. Xia, *Nat. Protoc.*, 2007, **2**, 2182–90.

13 N. Doshi, A. S. Zahr, S. Bhaskar, J. Lahann and S. Mitragotri, *P. Natl. Acad. Sci. USA*, 2009, **106**, 21495–9.

14 C. J. Murphy, T. K. Sau, A. M. Gole, C. J. Orendorff, J. Gao, L. Gou, S. E. Hunyadi and T. Li, *J. Phys. Chem. B*, 2005, **109**, 13857–70.

15 S. Mitragotri and J. Lahann, *Nat. Mater.*, 2009, **8**, 15–23.

16 P. F. Damasceno, M. Engel and S. C. Glotzer, *Science*, 2012, **337**, 453–7.

17 H. Yamakawa, *Modern Theory of Polymer Solutions*, Harper and Row, Publishers, New York, 1971.

18 J. F. Douglas, J. Roovers and K. F. Freed, *Macromolecules*, 1990, **23**, 4168–4180.

19 C. Tanford, *Physical Chemistry of Macromolecules*, John Wiley and Sons, New York, NY, 1961.

20 N. Elkies, A. Odlyzko and J. Rush, *Invent. Math.*, 1991, **105**, 613–639.

21 L. Rossi, S. Sacanna, W. T. M. Irvine, P. M. Chaikin, D. J. Pine and A. P. Philipse, *Soft Matter*, 2011, **7**, 4139.

22 Y. Jiao, F. Stillinger and S. Torquato, *Phys. Rev. E*, 2009, **79**, 041309.

23 R. D. Batten, F. H. Stillinger and S. Torquato, *Phys. Rev. E*, 2010, **81**, 061105.

24 R. Ni, A. P. Gantapara, J. de Graaf, R. van Roij and M. Dijkstra, *Soft Matter*, 2012, **8**, 8826–8834.

25 M. Marechal, U. Zimmermann and H. Löwen, *J. Chem. Phys.*, 2012, **136**, 144506.

26 S. Erdoğan, N. Martys, C. Ferraris and D. Fowler, *Cement Concrete Comp.*, 2008, **30**, 393–402.

27 C. Cañas Peñuelas, S. Catalan-Izquierdo, J. Bueno-Barrachina and F. Cavallé-Sesé, *Proceedings of the International Conference on Renewable Energies and Power Quality (ICREPQ09)*, 2009.

28 P. Zipper and H. Durchschlag, *Eur. Biophys. J.*, 2013, **42**, 559–73.

29 A. Sihvola, P. Yla-Oijala, S. Jarvenpaa and J. Avelin, *IEEE T. Antenn. Propag.*, 2004, **52**, 2226–2233.

30 J. H. Wang, *J. Am. Chem. Soc.*, 1954, **76**, 4755–4763.

31 A. Einstein, *Ann. Phys.*, 1911, **34**, 591 – 592.

32 J. F. Douglas and E. J. Garboczi, *Adv. Chem. Phys.*, John Wiley & Sons, Inc., Hoboken, NJ, USA, 1995, vol. 91, pp. 85–153.

33 G. Polya and G. Szegö, *Isoperimetric Inequalities in Mathematical Physics*, Princeton University Press, Princeton, NJ, 1951.

34 G. Polya, *Am. Math. Mon.*, 1947, **54**, 201.

35 J. B. Keller, R. E. Kleinman and T. B. A. Senior, *IMA Appl. Math.*, 1972, **9**, 14–22.

36 J. E. Martin and G. Gulley, *J. Appl. Phys.*, 2009, **106**, 084301.

37 J. E. Martin, K. J. Solis, D. Rademacher and V. Raksha, *J. Appl. Phys.*, 2012, **112**, 054306.

38 T. Kihara, *Rev. Mod. Phys.*, 1953, **25**, 831–843.

39 A. Isihara and T. Hayashida, *J. Phys. Soc. Jpn.*, 1951, **6**, 40–45.

40 M. Mansfield, J. Douglas and E. Garboczi, *Phys. Rev. E*, 2001, **64**, 061401.

41 J. Hubbard and J. Douglas, *Phys. Rev. E*, 1993, **47**, R2983–R2986.

42 S. R. Aragon and D. Flamik, *Macromolecules*, 2009, **42**, 6290–6299.

43 M. L. Mansfield and J. F. Douglas, *Phys. Rev. E*, 2008, **78**, 046712.

44 D. F. Calef and J. M. Deutch, *Ann. Rev. Phys. Chem.*, 1983, **34**, 493–524.

45 H.-X. Zhou, A. Szabo, J. F. Douglas and J. B. Hubbard, *J. Chem. Phys.*, 1994, **100**, 3821.

46 A. Friedman and J. Douglas, in *Mathematics in Industrial Problems*, Springer New York, 1995, vol. 67, pp. 166–185.

47 *ZENO*, http://web.stevens.edu/zeno/.

48 *COMSOL Multiphysics*, http://www.comsol.com/comsol-multiphysics.

49 Certain commercial equipment and/or materials are identified in this report in order to adequately specify the experimental procedure. In no case does such identification imply recommendation or endorsement by the National Institute of Standards and Technology, nor does it imply that the equipment and/or materials used are necessarily the best available for the purpose.

50 J. E. Martin, E. Venturini, J. Odinek and R. A. Anderson, *Phys. Rev. E*, 2000, **61**, 2818–2830.

51 *SCUFF-EM*, http://homerreid.com/scuff-EM.

52 *Mathematica 8.0*, 2010.

53 A. Russell, *Journal IEE*, 1916, **55**, 1–17.

54 J. E. Martin, E. Venturini, G. L. Gulley and J. Williamson, *Phys. Rev. E*, 2004, **69**, 021508.

55 In Ref. 54, $[\sigma]_\infty$, can be determined from the reciprocal of the demagnetization factor, which was reported as 0.27440.

56 R. K. Mallavajula, D. L. Koch and L. A. Archer, *Phys. Rev. E*, 2013, **88**, 052302.

57 J. Singh and D. Kofke, *Phys. Rev. Lett.*, 2004, **92**, 220601.

58 J. R. Royer, G. L. Burton, D. L. Blair and S. D. Hudson, In preparation.

59 S. H. Ko, F. Vargas-Lara, P. N. Patrone, S. M. Stavis, F. W. Starr, J. F. Douglas and J. A. Liddle, *Soft Matter*, 2014, **10**, 7370–7378.

60 C. R. Snyder and J. F. Douglas, *J. Phys. Chem. B*, 2000, **104**, 11058–11065.

61 H. Brenner, *Chem. Eng. Sci.*, 1964, **19**, 519–539.

62 J. F. Douglas and K. F. Freed, *Macromolecules*, 1994, **27**, 6088–6099.

63 R. M. Venable and R. W. Pastor, *Biopolymers*, 1988, **27**, 1001–1014.